Quantifying Wave Setup Climatology along the U.S. East and Gulf Coasts using a Coupled Hydrodynamic-Wave Model

ASM Alauddin Al Azad[a] and Reza Marsooli[a]

[a] Department of Civil, Environmental, and Ocean Engineering, Stevens Institute of Technology, Hoboken, NJ 07030, United States

Corresponding author: Reza Marsooli, rmarsool@stevens.edu

ABSTRACT

Wave setup, the increase in coastal mean water level due to wave breaking, is an important but understudied component of coastal sea-level long-term variability. This study quantifies the wave setup climatology along the U.S. East and Gulf of Mexico coasts using high-resolution hydrodynamic (ADCIRC) and wave (SWAN) models. The models are forced with hourly surface pressure and wind fields, total water level, and direction–frequency wave spectra from the ERA5 reanalysis dataset. We conduct decade-long (2006-2015) simulations to quantify the mean and extreme (99^{th} percentile) wave setups and characterize their interannual variabilities, spatial coherence, and trends. Results from 32 representative sites indicate that wave setup along the U.S. East Coast is generally larger than that along the Gulf Coast. Seasonally, winter months exhibit higher mean and extreme wave setup than summer months on both coasts. Interannual variability of the annual mean and extreme wave setup is, respectively, 57% and 28% larger on the East Coast than on the Gulf Coast. We find that wave-setup anomalies show strong coherence at short alongshore separations (0–75 km) along both coasts, but remain spatially correlated over much longer distances on the East Coast (decorrelation range 642 km) than in the Gulf (292 km). Finally, trend analysis reveals mixed positive and negative trends in wave setup along the East Coast and predominantly negative trends in the Gulf.

Key Words: wave setup, dynamic modeling, long-term trends, ADCIRC, SWAN

1. Introduction

Quantifying long-term variations in coastal sea level conditions is essential for understanding and enhancing coastal resilience. Spatial and temporal variability as well as trends in coastal sea levels are important factors in shaping flood hazards, coastal erosion, and ecosystem dynamics. Coastal sea level climatology is influenced by various components across a range of timescales and spatial scales from local to global, i.e., tides, atmospheric surges, wind-induced waves, and river runoff (Woodworth et al., 2019). Understanding the climatological behavior of these components, including their mean, variability, and long-term trends, is therefore fundamental for improving coastal hazard assessments and developing effective adaptation strategies.

Among coastal processes, wind-generated waves are a critical yet often underappreciated contributor to coastal sea level variability and change (Melet et al., 2018). Wind-generated

waves are composed of both locally generated waves (i.e., wind seas) and remotely generated waves that have traveled out of the generating area (i.e., swells). On exposed coasts, wave-induced processes govern the nearshore dynamics and modulate coastal water level. Among these processes is wave setup, the increase in the mean water level that occurs when waves break in the surf zone, as the waves' momentum is transferred to the water, elevating the local water surface (Longuet-Higgins and Stewart, 1962; Bowen et al., 1968). The amplitude of wave setup is generally pronounced during storms and can significantly increase water levels along the coast. On sandy coasts, wave setup generally amounts to about 10–20% of the breaking wave height, and during intense storms it can exceed 1 m and, therefore, become an important contributor to the storm surges (Pedreros et al., 2018; Dodet et al., 2019). Along the U.S. East and Gulf of Mexico coasts, despite the wide continental shelf, wave setup is significant during storms (Marsooli et al., 2017), contributing up to 17% of peak storm tides generated by historical tropical cyclones (Marsooli and Lin, 2018). On narrow-shelf segments, wave setup can reach up to 50% of the total 100-year surge (Dean et al., 2005). While the contribution of wave setup to sea levels at a storm time scale is extensively studied, our understanding of its effects on long-term sea level change and variability is limited.

The limited number of studies on the long-term climatology of wave setup is partly due to constraints imposed by current observational systems. Contemporary sea-level variability is primarily monitored using satellite radar altimetry and coastal tide gauges. However, neither platform directly measures the wave setup. Satellite altimeters have provided continuous, near-global measurements at a few-day interval since the late 1990s (Li et al., 2016), but they measure only offshore sea surface height and significant wave height. One approach to estimate wave setup is to utilize both satellite altimetry and local tide gauge data. In this method, the collocated altimetry-derived offshore sea surface height is subtracted from the coastal tide gauge water level, isolating the local wave setup component (Ray et al., 2022). However, this approach is primarily applicable in regions where wave effects dominate the local tide gauge signal. Although tide gauges provide long-term records of water levels, with some extending back to the eighteenth century, they are typically located in sheltered harbors where wave impact is minimal. As a result, combining altimetry and tide-gauge measurements can yield wave setup estimates at only a few locations worldwide. Moreover, satellite altimetry has limited near-coastal coverage, although recent advances have extended measurements to within 1–2 km of the shoreline (Birol et al., 2021; Schlembach et al., 2023).

Field measurements have been utilized to directly measure wave setup using in-situ pressure gauges. For example, Raubenheimer et al. (2001) deployed twelve buried pressure sensors along a cross-shore transect from the shoreline to about 5 m water depth to record bottom pressure variations. The mean water level derived from these sensors was compared across the transect, and the increase in mean water level toward the shore relative to the offshore sensor was interpreted as the wave setup. However, long-term deployment of in situ measurement instruments is difficult due to intense wave-energy dissipation, strong currents, and rapid morphological change that disrupt pressure sensors and data continuity (Melet et al., 2016). Consequently, direct observations of wave setup are usually obtained through intensive in-situ measurements that span only from several days to weeks (e.g., Heidarzadeh et al., 2009), which prevents the collection of long-term records needed to evaluate wave-setup climatology.

Empirical and computational methods for wave setup calculation have become available over the past decades, which resulted in the emergence of regional to global scale studies accounting for wave contributions to coastal sea levels (Vitousek et al., 2017; Woodworth et al., 2019; Ruggiero 2013; Dodet et al., 2019; Haasnoot et al., 2021). For instance, Melet et al. (2018) used an empirical wave setup formulation to conduct a first-order, global-scale estimate of the contribution of wave setup and swash to coastal sea level variability on interannual to decadal timescales. Their results indicate that wave-induced contribution to interannual-to-multidecadal total water level changes is significant over large parts of the global coastline, with a median contribution of ~58% across 153 sites over the last two decades. Melet et al. (2020) extended this analysis to future scenarios, evaluating 20-year mean wave setup changes at the mid- and end-21st-century. They found that wave setup changes tend to cancel out when averaged globally, but at regional or local scales, even a modest change in wave setup can be significant relative to other contributors to coastal sea-level change (e.g., glacial isostatic adjustment and land-water transfer). This underscores the need to incorporate wave dynamics into regional sea-level change assessments to improve the accuracy of coastal flooding and erosion predictions.

Current studies on the long-term effect of wave setup on sea level changes, such as the abovementioned studies, are often criticized for relying on empirical formulations based on the deep-water wave energy flux, nearshore profile, beach slope, and morphological conditions (Dodet et al., 2019). Since the estimated wave setup based on the empirical

formulations is sensitive to beach slope and the chosen formulation, site-specific geomorphic data are important for reducing error. However, there is a lack of detailed foreshore survey data at regional to global scales. As a result, many studies adopt a constant beach slope (e.g., Melet et al., 2018; Melet et al., 2020; Serafin et al., 2017) or infer a constant slope value from standard sediment grain sizes (Rueda et al., 2017). Moreover, empirical formulations are derived from limited field measurements (Holman & Sallenger, 1985; Stockdon et al., 2006; Atkinson et al., 2017), which can limit their applicability across diverse coastal settings (Aucan et al., 2019). Alternatively, despite their higher computational demands, dynamical modeling of wave setup using coupled hydrodynamic-wave models is considered an accurate approach (Camus et al., 2013) for resolving the complex physical process in coastal waters that influence wave setup, e.g., wave refraction and breaking, and wave-current interactions.

To this end, the goal of this study is to advance understanding of the climatology of wave setup along the U.S. East and Gulf of Mexico coasts using a dynamical approach. To achieve this goal, we perform and compare coastal sea level simulations using a stand-alone hydrodynamic model (i.e., neglecting wave effects) and a coupled hydrodynamic-wave model (i.e., accounting for wave effects) over a 10-year period from 2006 to 2015. Using the simulated wave setup estimates, statistical analyses are performed to quantify the 10-year mean wave setups, their spatial and temporal (monthly, seasonal, and interannual scales) variation, and trends.

2. Methodology

2.1. Coupled Hydrodynamic and Wave Model

We employ the regional-scale coupled hydrodynamic-wave model validated by Al Azad and Marsooli (2024) to generate wave setup estimates along the U.S. East and Gulf coasts for the period of 2006-2015. This model uses ADCIRC and SWAN as its hydrodynamic and wave models, respectively. ADCIRC (Luettich et al. 1992; Westerink et al. 1994) solves the depth-averaged barotropic form of the shallow water equations for the calculation of long-period waves such as astronomical tides and storm surges. SWAN (Booij et al., 1999; Ris et al., 1999) is a third-generation spectral wave model that solves the depth-integrated wave-action balance with source and sink terms for wind input, whitecapping, bottom friction, nonlinear interactions, and depth-limited breaking.

In the coupled ADCIRC+SWAN modeling system, the hydrodynamic and wave components exchange time-varying fields to represent two-way wave–current–water level interactions on a common unstructured mesh (Dietrich et al., 2011, 2012). Specifically, ADCIRC passes the calculated water levels and currents to SWAN. These quantities are utilized by SWAN to account for wave–current interactions and the influence of evolving nearshore water depth on wave transformation processes such as refraction, shoaling, and dissipation (Luettich et al., 1992; Westerink et al., 1994; Booij et al., 1999; Ris et al., 1999). SWAN subsequently computes the wave radiation stresses and their gradients (Longuet-Higgins and Stewart, 1964; Dietrich et al., 2011, 2012) at the end of each of its time steps, and these gradients are passed back to ADCIRC as a wave-induced forcing function in the depth-averaged momentum equations (Dietrich et al., 2011, 2012). This two-way coupling modifies the hydrodynamic momentum balance and the water surface elevation, enabling the explicit representation of wave-induced forcing on coastal water levels. This coupling approach is well established and widely used in storm surge and coastal hazard modeling. Details of the governing equations, coupling procedure, and interaction scheme for the ADCIRC and SWAN models are provided in the literature (e.g., Dietrich et al., 2012; Marsooli and Lin, 2018; Al Azad and Marsooli, 2024).

The computational domain developed by Al Azad and Marsooli (2024), which covers the western North Atlantic Ocean between latitudes 6°N and 46°N and longitudes 98°W and 53°W, is discretized using an unstructured mesh. The mesh resolution is 500 m to 1 km in coastal waters up to a water depth of 300 m, transitions to 5 km up to a water depth of 1000 m, and gradually increases to 20 km in deep waters. The bathymetry of the model domain is based on GEBCO 2021. This unstructured mesh is used in both ADCIRC and SWAN models. In SWAN, the spectral domain is discretized into 36 directional bins and 31frequencies, spanning 0.04–0.667 Hz.

2.2. Forcings

We force stand-alone ADCIRC and the coupled ADCIRC + SWAN models with the same atmospheric forcing. The models are forced using hourly surface pressure and 10-m wind fields from the ERA5 reanalysis dataset (Hersbach et al., 2020), which has a horizontal resolution of 0.25°×0.25°. The models are also forced along their open-ocean boundary with water levels from ERA5. In ADCIRC+SWAN simulations, we additionally force the SWAN model at its open-ocean boundary with direction-frequency wave spectra from ERA5, which

has spectral resolutions of 24 directional bins and 30 frequency bins, and a spatial resolution of 0.5° × 0.5°. The inclusion of wave boundary conditions in SWAN accounts for incoming swells generated outside the computational domain.

The validated ADCIRC model utilizes a quadratic bottom friction coefficient of 0.0035, and internal-tide conversion is represented with a non-local parameterization (scale factor 2.9; minimum cutoff depth 100 m). The validated SWAN model employs the ST6 source-term package with a combination of parameterization, including the power coefficient of local dissipation (p1sds = 4), power coefficient of cumulative dissipation (p2sds =4), local dissipation term (a1sds = 6.5E-6), cumulative dissipation term (a2sds = 8.5E-5), factor to scale the U10 with U* (windscaling = 35), and swell dissipation based on the Ardhuin et al. (2010). Bottom-friction dissipation is represented with the JONSWAP formulation, using a constant coefficient of 0.038 m^2/s^3.

We conducted our simulation on the Purdue University Anvil high-performance computing system through an allocation supported by NSF ACCESS (Boerner et al., 2023). A 31-day ADCIRC+SWAN simulation required about 26 h on the Anvil CPU partition using two compute nodes; each node is powered by two 64-core AMD EPYC "Milan" processors with 128 computational cores and 256 GB RAM.

2.3. Estimation of Wave Setup

We calculate wave setup along the coast by comparing simulated water levels from two series of simulations: fully coupled ADCIRC+SWAN (hereafter "with-wave") and stand-alone ADCIRC (hereafter "no-wave"). The with-wave simulations include the effect of wave radiation stress and, thus, wave setup on water levels, while the no-wave simulations exclude wave effects.

At each time step and coastal site, wave setup is quantified as the difference in the modeled water level between these two simulations:

$$\eta_{wave\ setup}(x, y, t) = \eta_{with-wave}(x, y, t) - \eta_{no-wave}(x, y, t) \quad (1)$$

Here, $\eta_{with-wave}$ is the water level (tide + surge + wave effects) from the coupled ADCIRC+SWAN model, and $\eta_{no-wave}$ is the water level (tide + surge) from the stand-alone ADCIRC model. This difference isolates the increase in water level attributable to the wind-generated waves at each site (x, y), and each time step (t). This approach of using paired simulations to estimate wave setup has been employed in previous studies (Dietrich et al.,

2011; Marsooli and Lin, 2018) and ensures that wave setup is evaluated under identical tidal and meteorological conditions.

2.4. Sites along the U.S. East and Gulf Coasts

To present the variation in wave setup along the coastline, 32 representative coastal sites are selected for analysis. Fig. 1 and Table 1 present the locations of these sites along the U.S. East and Gulf of Mexico coasts. The sites span the Northeast and Mid-Atlantic coast (sites 1–8; from New York through Virginia), the Southeast Atlantic coast (sites 9–17; covering the Carolinas down to Florida's east coast), and the Gulf of Mexico (sites 18–32; from the Florida Gulf Coast westward to Texas). This broad distribution ensures that different coastal environments and wave climate conditions are represented in the analysis.

The coastal sites correspond to the model grid cells nearest to the shoreline and areas where the nearshore bathymetric gradient is smooth. Our criterion for selecting these sites is that the nearshore bathymetric gradient is gentle or smooth rather than abrupt. A gradual bathymetric slope allows waves to increase in height (shoaling) and then break successively, causing energy dissipation over a wide surf zone. Accordingly, we selected sites where the surf zone is relatively wide, and the model mesh consists of more than two nodes across the surf-zone width. As a result, the wave momentum flux, and thus the radiation stress, decreases smoothly shoreward, producing a well-resolved radiation stress gradient in the ADCIRC+SWAN model. In contrast, steep or irregular bathymetry confines wave breaking to a narrow zone, creating sharp radiation stress gradients, strong wave reflections, and greater numerical sensitivity. Accurately resolving the radiation stress and capturing the wave setup under such steep conditions requires ultra-high-resolution numerical models, i.e., about 10 grid points per surf-zone width. In regional-scale, long-term wave setup studies, such as the present study, ultra-high-resolution modeling is computationally expensive. Accordingly, we excluded the Gulf of Maine from our analysis because its nearshore bathymetry is steep and highly heterogeneous, with a bedrock-framed shelf punctuated by deep basins and ridges shaped by Pleistocene glacial erosion and post-glacial processes (Belknap et al., 2002).

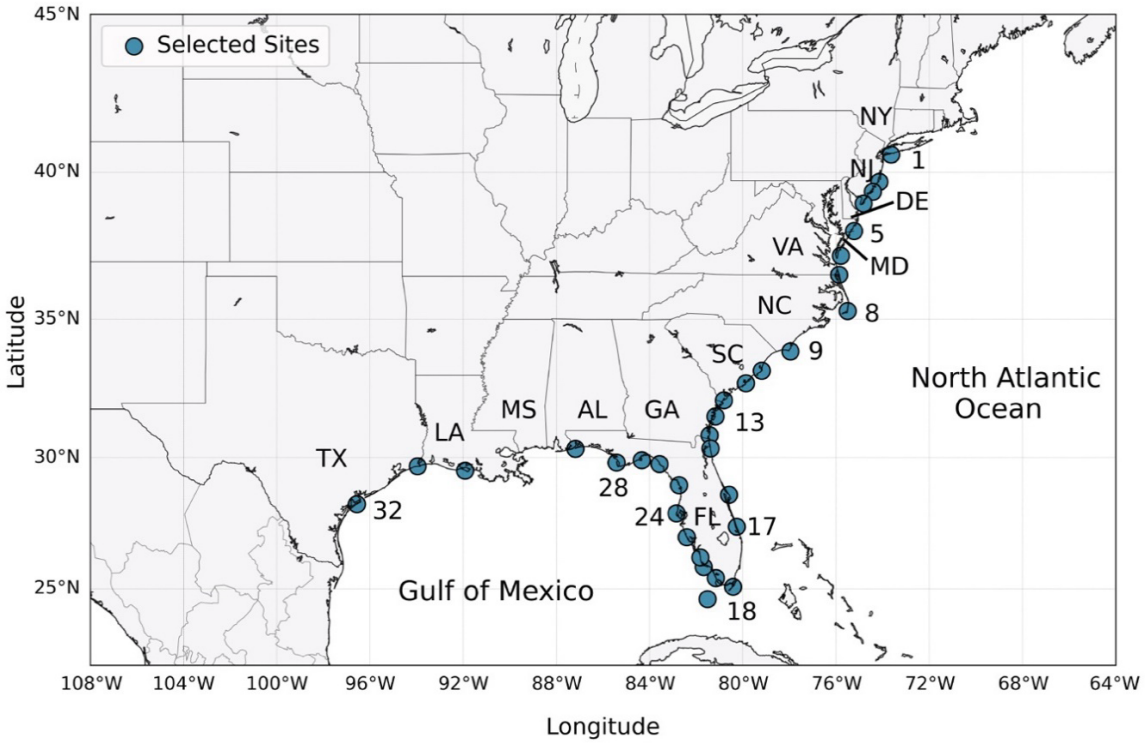

225

226 Fig. 1. Location of the 32 selected coastal sites to present the variation in wave setup
227 along the U.S. East and Gulf of Mexico coasts.

228 Table 1. Location of the selected sites along the U.S. East and Gulf of Mexico coasts.

Site	Longitude	Latitude	Site	Longitude	Longitude
1 (Long Beach, NY)	-73.642369	40.5826	17 (Fort Pierce, FL)	-80.259217	27.399237
2 (Surf City, NJ)	-74.144326	39.687555	18 (Key Largo, FL)	-80.420795	25.08855
3 (Atlantic City, NJ)	-74.415583	39.360348	19 (Sugarloaf Key, FL)	-81.517478	24.609988
4 (Wildwood, NJ)	-74.82515	38.973043	20 (Everglades City, FL)	-81.161939	25.428671
5 (Chincoteague, VA)	-75.228611	38.043146	21 (Marco Island, FL)	-81.683398	25.851955
6 (Cape Charles, VA)	-75.801007	37.209284	22 (Naples, FL)	-81.823077	26.225506
7 (Virginia Beach, VA)	-75.867867	36.554843	23 (Englewood, FL)	-82.408904	26.995508
8 (Buxton, NC)	-75.509755	35.291218	24 (Clearwater, FL)	-82.849768	27.910559
9 (Wrightsville Beach, NC)	-77.956667	33.862523	25 (Crystal River, FL)	-82.740098	28.968974
10 (Georgetown, SC)	-79.188774	33.173258	26 (Steinhatchee, FL)	-83.580645	29.757835
11 (Charleston, SC)	-79.870378	32.725578	27 (Alligator Point, FL)	-84.33803	29.899988
12 (Hilton Head Island, SC)	-80.810396	32.103884	28 (Mexico Beach, FL)	-85.418126	29.811898
13 (Brunswick, GA)	-81.178581	31.518665	29 (Pensacola Beach, FL)	-87.188561	30.324769
14 (Fernandina Beach, FL)	-81.431516	30.83188	30 (Cypremort Point, LA)	-91.923684	29.515274
15 (Jacksonville Beach, FL)	-81.393017	30.339768	31 (Sabine Pass (Port Arthur), TX)	-93.959018	29.676111
16 (Cape Canaveral, FL)	-80.59247	28.609759	32 (Port O'Connor, TX)	-96.563058	28.257419

229

2.5. Statistical metrics

Using the estimated wave setup time series, various statistical analyses are performed to quantify wave setup climatology over the 10-year period of 2006–2015. We calculate a mean wave setup at each site by averaging the wave setup values at that site over the entire 10-year span. Similarly, we quantify the extreme wave setup at each site as the 99^{th} percentile of the wave setup estimates during the study period. These metrics establish the mean and extreme levels of wave-induced water level increase at each site.

In order to assess temporal variation in wave setup at each site, we further analyze the calculated time series of wave setup at seasonal and monthly time scales. The wave setup data is grouped into two extended seasons, winter (October–March) and summer (April–September), to compute the seasonal statistics. For each site, all wave setup estimates corresponding to winter months from 2006 to 2015 are aggregated to calculate the winter mean and extreme wave setup. Similarly, the summer mean and extreme wave setup are obtained by aggregating all wave setup estimates from the summer months over the same 10-year period. For the monthly analysis, we similarly aggregate the wave setup estimates by calendar month over the 10-year period and calculate the mean and extreme wave setup for each month at each site. The monthly and seasonal wave setups allow for identifying the sub-seasonal and seasonal patterns in mean and extreme wave setups.

To quantify interannual variability in wave setup, annual values and their standard deviation are calculated from the detrended wave setup estimates over the 10-year period. The detrended wave setup estimates are used to remove long-term changes and isolate year-to-year fluctuations. For each site and each year, the annual mean and extreme (99^{th} percentile) wave setups are computed from the detrended estimates. The interannual variability is then evaluated by computing the standard deviation of the annual mean and extreme values across the study period. A higher standard deviation signifies that the wave setup at that site experiences larger year-to-year fluctuations. This analysis reveals the year-to-year consistency of the mean and extreme wave setup at each location.

To investigate trends in wave setup between 2006 and 2015, we perform an Ordinary Least Squares (OLS) linear regression for each site. The resulting trend, slope of the regression line, provides the estimated rate of change in wave setup. Along with trend magnitude, its statistical significance is also evaluated using the regression's p-value, with a threshold of 0.05 for 95% confidence, to evaluate the robustness of trends in wave setup.

2.6. Spatial coherence and spatial dependence

To determine the spatial scale over which wave-setup variability is regionally coherent and to assess how rapidly wave-setup similarity decays with distance, we quantify the distance dependence of monthly wave-setup anomalies. For each site, a monthly anomaly time series is computed by subtracting the site-specific long-term mean over 2006-2015 from the monthly mean wave setup estimate, so that the analysis reflects coherent departures from typical conditions. Inter-site separation distances are computed as great-circle (haversine) distances from site coordinates, and all unique site pairs were considered.

We estimate spatial coherence from the pairwise Pearson correlation coefficient (r) between anomaly time series of wave setup at site pairs. Pearson r provides a standardized measure of linear co-variability bounded between −1 and +1, where positive values indicate that anomalies tend to vary in the same direction across sites and negative values indicate opposing variability. The spatial correlogram is constructed by associating each pairwise correlation value with the corresponding inter-site distance.

Spatial dependence is characterized using the omnidirectional experimental semi-variogram, defined as half the mean squared difference between anomaly values at site pairs separated by distance h (Cressie, 1993) as follows:

$$\hat{\gamma}(h) = \frac{1}{2n(h)} \sum_{k=1}^{n(h)} [\acute{z}(x_{i_k}, t) - \acute{z}(x_{j_k}, t)]^2 \quad (2)$$

Here, $n(h)$ is the number of site pairs whose separation distance falls within the distance class centered on h, and (i_k, j_k) denotes the k-th site pair in that distance class. x_i and x_j are, respectively, the geographic locations of sites i and j, and $\acute{z}(x_{i_k}, t)$ presents the monthly wave-setup anomaly at site i_k for month t. With the simulated wave setup at n coastal sites, the number of unique site pairs is $n(n-1)/2$; thus, for the U.S. East Coast (n = 17) this yields 136 inter-site pairs, and for the Gulf of Mexico (n = 15) yields 105 inter-site pairs. As inter-site separations are discrete and unevenly distributed, we aggregate semi-variance estimates within distance classes (lags). Distances are grouped using 75-km bins up to 750 km and 200-km bins beyond 750 km, to maintain adequate sample sizes. The mean semi-variance in each class is used to represent $\hat{\gamma}(h)$. Since the binned semi-variogram provides discrete estimates, a parametric model can be fitted to obtain a compact description of spatial dependence. In this study, we adopt a spherical variogram model, which provides the

representation of the distance dependence of wave setup anomalies (Berne et al., 2004). The spherical variogram model is characterized by the sill, defined as the plateau (maximum) semi-variance reached at large separation distances, and the range, defined as the characteristic distance at which the semi-variance approaches the sill and the anomalies become effectively uncorrelated.

3. Results

3.1. Mean and Extreme Wave Setup

Fig. 2 illustrates the spatial distribution of mean and extreme wave setups. Overall, sites along the U.S. East Coast exhibit substantially higher mean and extreme wave setups than sites along the Gulf of Mexico. For example, the Northeast and Mid-Atlantic region (sites 1-8) has the largest wave setup, with mean and extreme wave setups of 0.8–1.47 cm and 5.0 – 8.2 cm, respectively. The Southeast Atlantic (sites 9–17) shows intermediate wave setup values with large spatial variability, with mean and extreme values of 0.47–1.68 cm and 3.2–8.0 cm, respectively. Along the entire East coast, the largest mean wave setup is 1.7 cm at site 10 located in South Carolina (SC), and the highest extreme wave setup is 8.2 cm at site 7 in Virginia (VA).

In contrast to the East Coast, wave setups at the sites in the Gulf of Mexico (sites 18-32) show much lower values; mean wave setup is within the range of 0.2–1.0 cm, and the extremes are between 1.5 and 4.7 cm. The largest wave setup across the study sites along the Gulf Coast is at site 32, on the westernmost side of the Gulf, with mean and extreme wave setups of 1.0 cm and 4.7 cm, respectively.

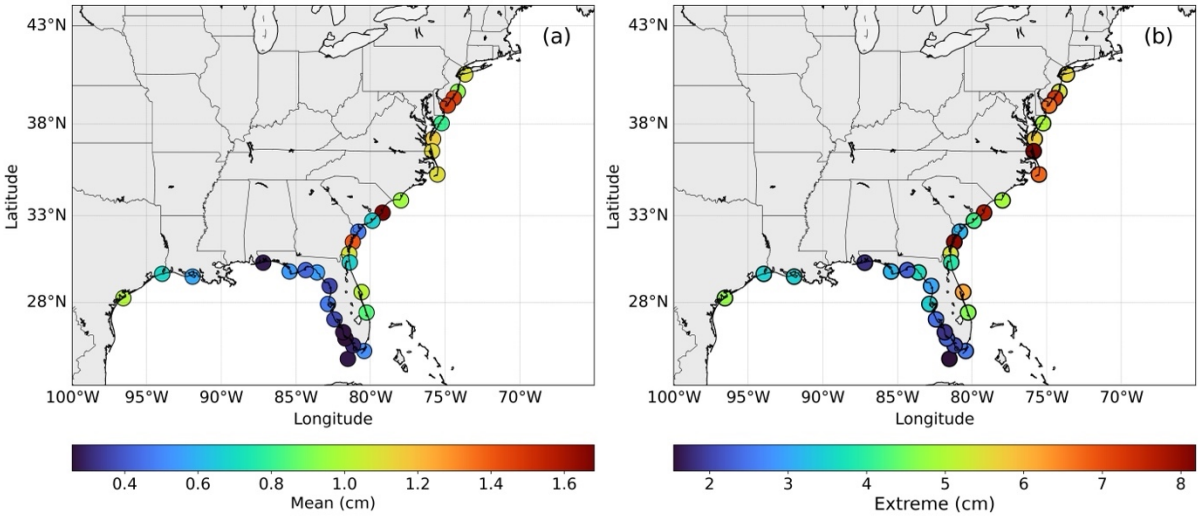

312

313 Fig. 2. Distribution of wave setups along the coast over a 10-year period between 2006
314 and 2015. (a) mean and (b) extreme (99th percentile) wave setup.

315 **3.2. Seasonal Mean and Extreme Wave Setup**

316 Fig. 3 demonstrates that both mean and extreme wave setups during winter are
317 substantially larger than in summer. In the Northeast and Mid–Atlantic coast (sites 1–8),
318 summer mean wave setup ranges from 0.6 to 1.1 cm, with an average of 0.9 cm, whereas
319 winter mean wave setup ranges from 1.0 to 1.8 cm, averaging 1.4 cm. This increase in mean
320 wave setup during winter is evident throughout all sites in this region. The Southeast Atlantic
321 region (sites 9–17) shows a similar pattern, with mean wave setup ranging from 0.4 to 1.5 cm
322 in summer (average 0.8 cm) and 0.5 to 1.8 cm in winter (average 1.1 cm). At sites in the Gulf
323 (18–32), the mean wave setup during summer ranges from only 0.1 to 0.9 cm (average
324 0.36 cm), whereas winter means range from 0.3 to 1.1 cm (average 0.55 cm). Seasonal
325 differences remain evident also for the extreme wave setup across the U.S. East and Gulf of
326 Mexico coasts (Fig. 3(c, d)), with much larger wave setup during winter.

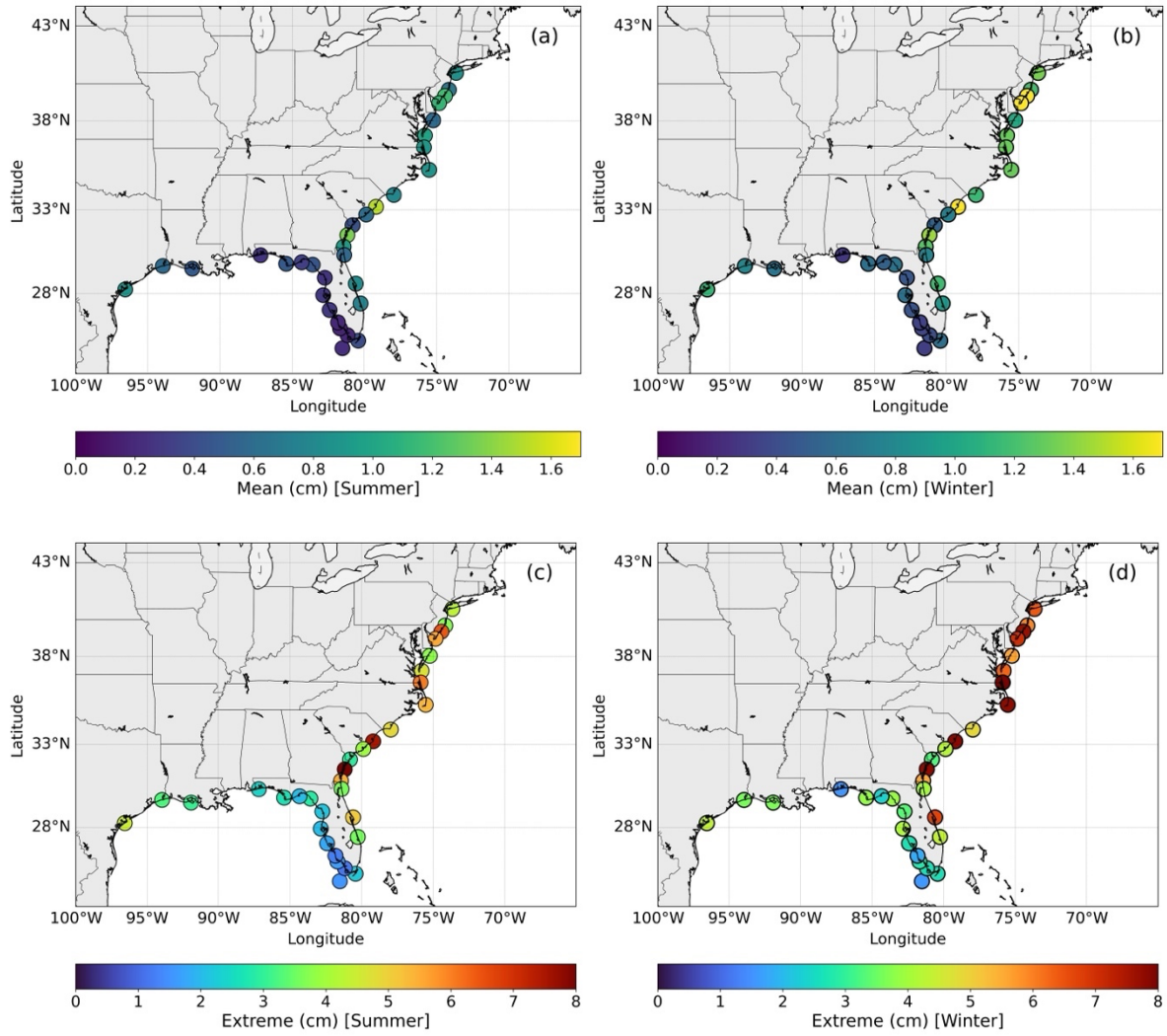

Fig. 3. Seasonal distribution of wave setup. (a) summer mean, (b) winter mean, (c) summer extreme (99th percentile), and (d) winter extreme (99th percentile) wave setup.

3.3. Monthly Mean and Extreme Wave Setup

The month-to-month variation of mean and extreme wave setup across 32 sites is shown in Fig. 4. Regionally, only a slight contrast emerges in month-to-month wave setup behavior between the Atlantic and Gulf coasts. The Atlantic sites (1-17) generally reach their highest magnitudes in November, whereas the Gulf Coast sites (18-32) peak slightly later in December. For example, along the Atlantic coast (site 10), the monthly mean wave setup reaches 2.3 cm in November, the largest observed, while the Gulf's maximum mean (1.3 cm, at site 32) occurs in December. Conversely, July exhibits the lowest mean and extreme wave setup at all sites, reflecting the mid-summer quiescence in wave activity. Consistent with the seasonal variation, late-season tropical cyclones overlapping with the onset of winter extratropical cyclones (e.g., nor'easters) intensify wave energy along the open Atlantic coast,

driving the late-Fall maximum in wave setup. Gulf Coast sites reach their highest wave setups in December, indicating a slight seasonal lag that is consistent with the dominance of winter cold-front systems.

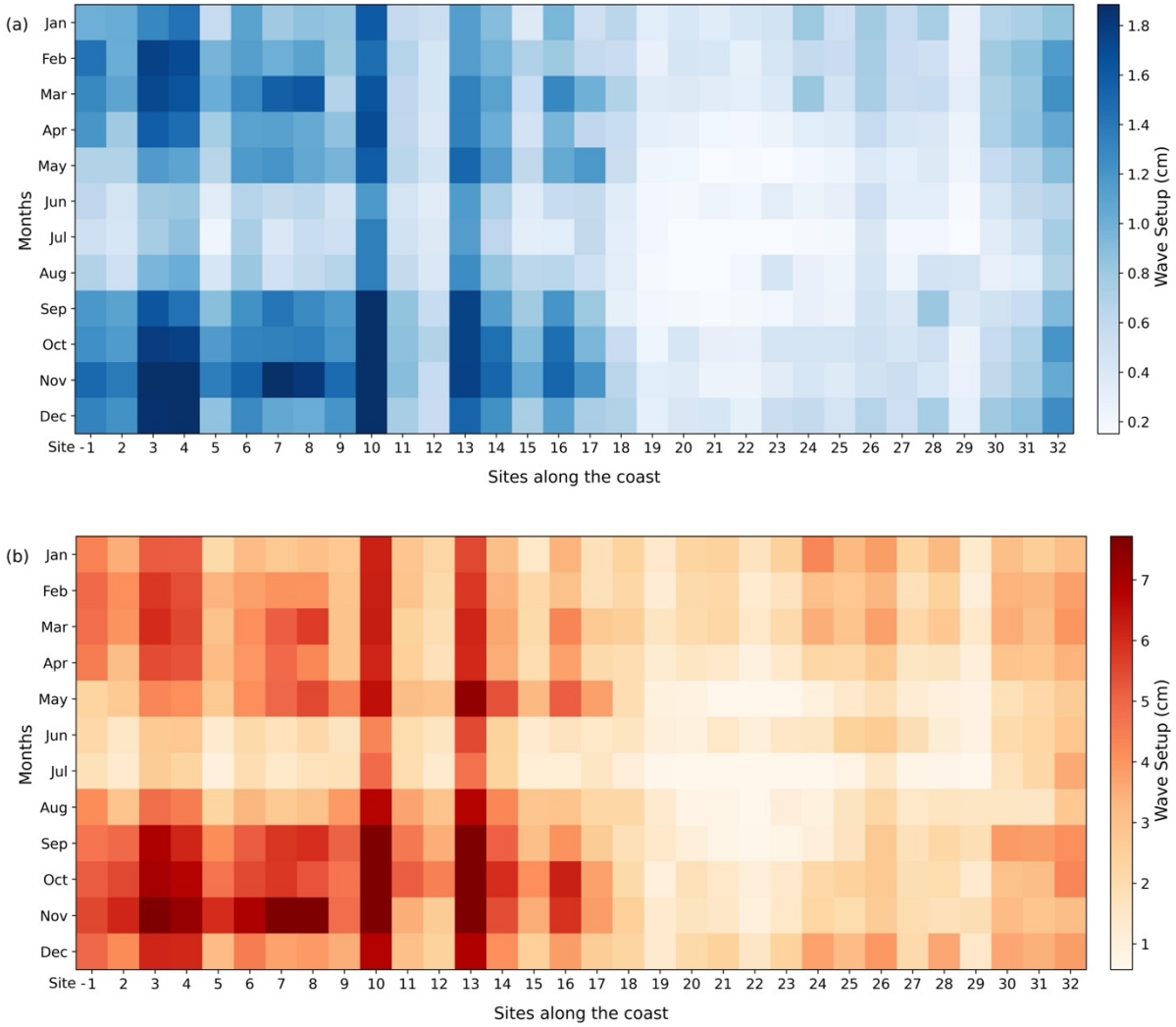

Fig. 4. Month-to-month variability of wave setup at study sites. (a) Monthly mean wave setup. (b) Monthly extreme (99th percentile) wave setup.

3.4. Interannual Variability

Fig. 5 shows the spatial variation in interannual variability in annual mean and extreme wave setups. The spatially averaged interannual variability of annual mean and extreme wave setup is, respectively, 0.11 and 1.09 cm along the Atlantic coast (sites 1-17), exceeding the averages (0.07 cm and 0.85 cm) of the Gulf coast (sites 18-33) by about 57% and 28%, respectively.

Across the Northeast Atlantic (sites 1–4), the average interannual variability in mean wave setup is 0.12 cm, reflecting year-to-year deviations driven by intense North Atlantic

353 storm forcing. The maximum interannual variability in annual mean wave setup in this region
354 is 0.15 cm, found at site 1 near the Long Beach, NY. The Mid-Atlantic (sites 5–8) also
355 exhibits high interannual variability in mean wave setup. In this region, the maximum value
356 of the variability metric (0.16 cm) is found at Site 8 near the Outer Banks of North Carolina
357 (NC).

358 Along the Southeast Atlantic coast (sites 9–17), interannual variability in annual mean
359 and extreme wave setup is higher at the central Florida (FL) sites compared with the Georgia
360 (GA) and South Carolina (SC) sites. For example, the highest interannual variability in the
361 annual mean wave setup of 0.17 cm is found at site 17 located in Fort Pierce, FL. For extreme
362 wave setup, interannual variability is highest at sites 16 and 17, with values of 1.77 and 1.72
363 cm. This area of the southeast Atlantic coast features a narrow continental shelf, leading to
364 wave breaking near the coast (Marsooli and Lin, 2018). The resulting high spatial gradients in
365 wave radiation stress generate a comparatively large wave setup. Thus, a slight change in
366 incident wave energy could result in a comparable change in wave setup. In contrast, the
367 lowest interannual variability in the annual mean wave setup in this region (southeast
368 Atlantic) is 0.03 cm at site 12. The interannual variability in the annual extreme wave setup at
369 this site is 0.72 cm, which is also the lowest along the U.S. East Coast. This area (Georgia,
370 South Carolina) of the Southeast coast has broad, shallow shelf that dissipates incoming
371 swells (Ardhuin et al., 2003), resulting in changing wave energy to have a relatively small
372 change in wave setup. The concave coastline further shelters this area from the impact of
373 large waves and thus their variability effects on wave setup.

374 The Gulf Coast (sites 18–32) exhibits lower interannual variability in wave setup than the
375 Atlantic Coast, with a few notable hotspots. Northwest Florida, especially the Panhandle
376 region (site 28), and the mid-Texas coast (site 32) stand out with higher year-to-year
377 deviations. For example, the highest interannual variability in the annual mean wave setup is
378 0.17 cm in this region, calculated at site 28 in the Florida Panhandle region. The interannual
379 variability in the annual extreme wave setup is 1.42 cm at this same site. This region often
380 lies in the crosshairs of landfalling hurricanes, so that an active storm year can elevate local
381 wave setup far above that of a quiet year. Additionally, Northwest Florida is influenced by
382 coastally trapped Kelvin waves (Lin et al., 2014), which are long-wavelength ocean waves
383 guided by the coastline that modify local sea levels and consequently wave conditions in
384 shallow waters. The highest interannual variability of the annual extreme wave setup is

calculated at site 32 (1.6 cm), reflecting this mid-Texas site's greater exposure to open-Gulf wave conditions. Overall, aside from these hotspots, most Gulf sites show relatively lower interannual wave setup, reinforcing the contrast with the more variable Atlantic coast.

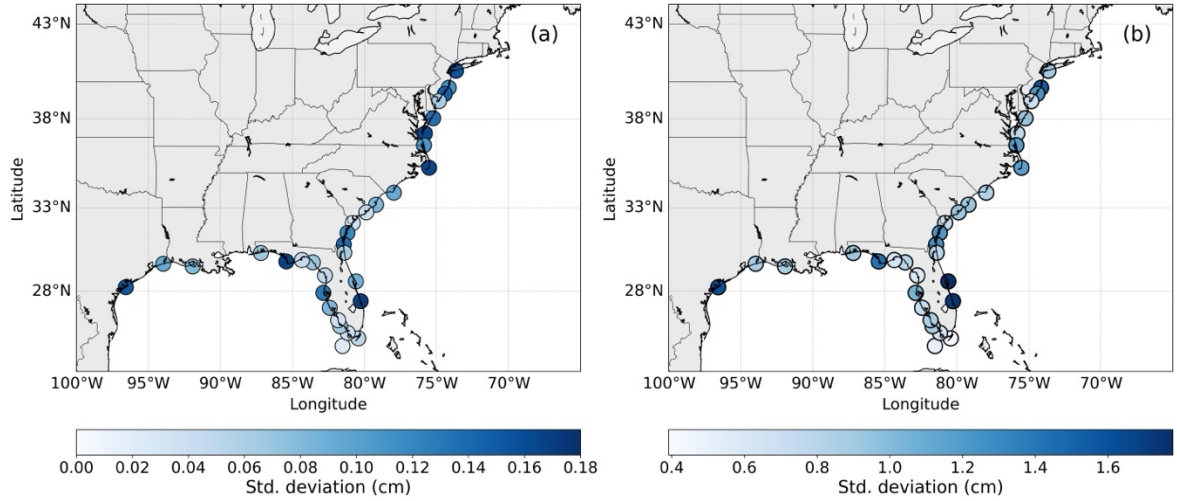

Fig. 5. Interannual variability in wave setup expressed as the standard deviation across annual statistics. (a) annual mean, (b) annual extreme (99th percentile) wave setups.

3.5. Spatial Correlation

Fig. 6 presents the Pearson spatial correlograms and semi-variograms of wave setup anomalies as a function of alongshore separation distance between site pairs. The spatial correlograms (Fig. 6 (a, b)) indicate that wave-setup anomalies are highly coherent at short alongshore separations on both East and Gulf coasts, but that the persistence of coherence with distance differs substantially between regions. Along the U.S. East Coast, mean pairwise Pearson correlations (r) are high at short separations and decay gradually with distance. The mean r is 0.69 within 0–75 km and remains above 0.5 through several hundred kilometers (e.g., 0.56 at 300–375 km), before weakening to 0.32–0.39 over the separation range of 600–1,150 km. Correlations remain positive even at the largest separations, suggesting that a basin-scale common forcing signal continues to influence wave setup anomalies along much of the U.S. East Coast, even as local site-specific variability increasingly modulates the response. In the Gulf Coast, correlations are also high at the shortest separations (mean r = 0.76 for 0–75 km), but coherence decreases more rapidly compared to the U.S. East Coast. For example, the mean r is 0.76 for 0–75 km, but declines to 0.57 over 75–225 km and further weakens to 0.45 at 225–300 km. At intermediate-to-long distance separations, the correlations are generally moderate (mean r is 0.42 for 675–750 km, and 0.39 for 950–1,150 km), and coherence is reduced at the largest distances (mean r is 0.25 for 1,350–1,559 km),

with greater dispersion among pairs as indicated by comparatively broad confidence intervals in several distance bins.

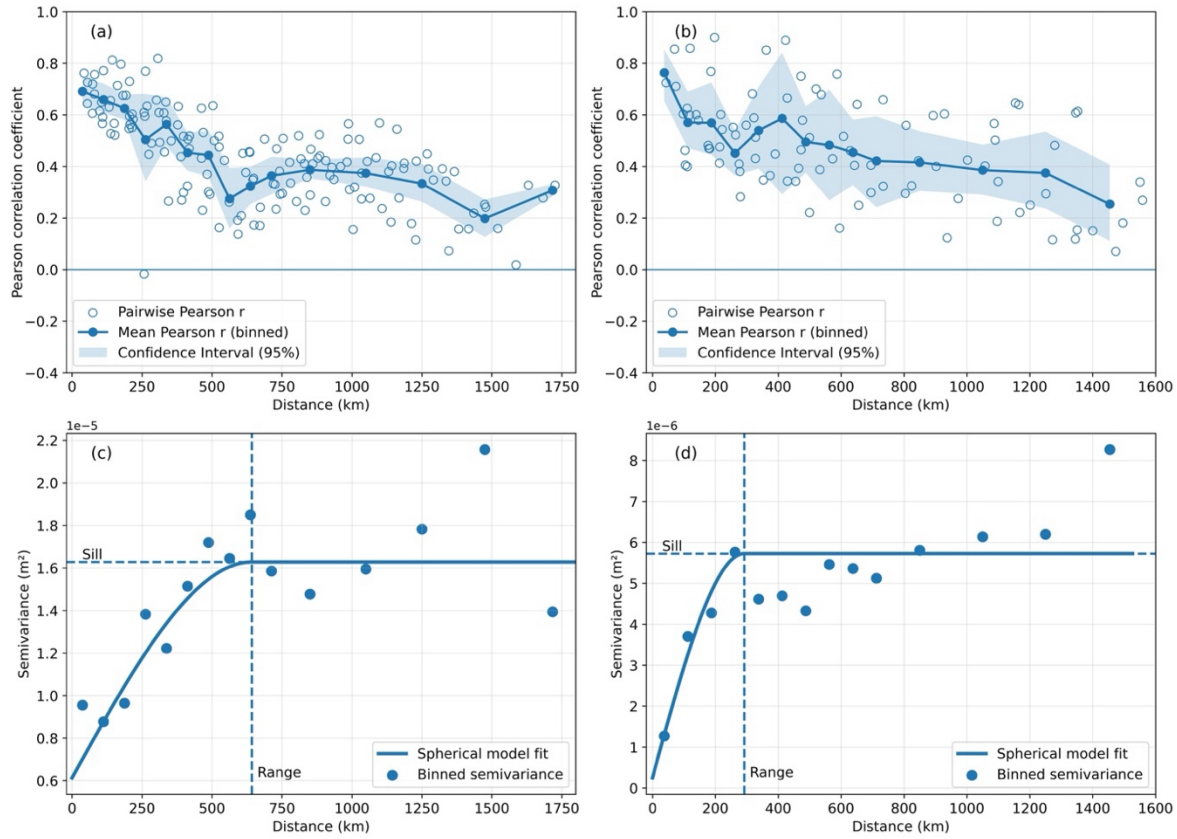

Fig 6. Spatial correlograms and semi-variograms of monthly wave-setup anomalies along the U.S. East (a, c) and Gulf of Mexico (b, d) coasts. Panels (a, b) show mean pairwise Pearson correlation versus alongshore separation distance, and panels (c–d) show binned empirical semi-variance with fitted spherical model.

The semi-variograms (Fig. 6 (c–d)) provide a complementary geostatistical characterization of spatial dependence by describing how semi-variance increases with separation distance and approaches a plateau as the wave setup field becomes effectively decorrelated. For the East Coast, the binned semi-variance increases from 0.9×10^{-5} m² at the smallest separations to values approaching $1.6–1.8\times10^{-5}$ m² over several hundred kilometers, and then approaches a plateau. The fitted spherical model indicates a decorrelation (range) scale of 642 km, beyond which additional separation does not systematically increase. In the Gulf Coast, semi-variance rises steeply over short separations and reaches its plateau much sooner; the spherical fit yields a substantially shorter range of 292 km and a lower sill value of 5.73×10^{-6} m².

Interpreted together with the correlograms, these ranges quantitatively reinforce that U.S. East Coast wave-setup anomalies maintain coherence over considerably larger distances than in the Gulf. These patterns suggest that the Atlantic coastline is more frequently influenced by large scale storm systems and swells that can impose coherent wave forcing over long stretches of coast, whereas the Gulf of Mexico is more influenced by local-to-regional controls (e.g., variable shelf width, bathymetry, coastal orientation, and geometry). Consequently, the Gulf Coast exhibits a shorter coherence length and earlier saturation of semi-variance, indicating a more rapid transition from regionally coherent variability to locally differentiated wave-setup behavior.

3.6. Trend

Fig. 7 shows trends in wave setup between 2006 and 2015, and their associated p-values. Among sites located in the Northeast and Mid-Atlantic region (sites 1-8), the highest trend in wave setup is found at site 7 (+0.30 mm/year) and the lowest trend is found at site 1 (−0.35 mm/year), with a regionally averaged trend of −0.02 mm/year. Most sites along the Southeast Atlantic coast (sites 9-17) show an increasing trend, with values ranging from +0.003 mm/year to +0.22 mm/year, and an average positive trend of +0.1 mm/year. Along the U.S. East coast, most sites show a p-value less than 0.05, suggesting the calculated trends are statistically significant, with only three sites (sites 9,10,11) in the southeast Atlantic coast fail to attain the statistical significance at the 95% confidence level. The results also show that trends in wave setup at sites along the Atlantic coast exhibit a mixed spatial pattern, in which adjacent sites often have opposite-signed trends, and there is no consistent pattern. For example, site 3 shows an increasing wave setup trend of +0.07 mm/year, while the nearby two sites, site 2 and 4, demonstrate decreasing trends of −0.08 and −0.03 mm/year, respectively. Consistent with our results, Jamous and Marsooli (2023) found substantial spatial variability in long-term trends of significant wave height along the U.S. East coast, attributing it to the combined influence of basin- to regional-scale forcing and site-specific factors (e.g., nearshore bathymetry, fetch length, local winds) that modulate nearshore wave conditions.

Across the Gulf region (sites 18-32), the wave setup trends are predominantly negative. Fig. 6 shows that negative wave setup trends cluster along the eastern Gulf. Trends at the Florida Keys/Straits sites (sites 18–21) range from −0.1 to −0.03 mm/year. The west Florida shelf (sites 23–27) shows uniformly negative trends in wave setup, with a maximum trend of

−0.19 mm/year at site 24 in this region. The Florida Panhandle shows the largest wave setup trend along the Gulf coast, with a value of −0.324 mm/year (site 28). Farther west, the Alabama–Louisiana shelf (sites 29–31) also exhibits downward trends, from −0.021 to −0.09 mm/year. An increasing trend is found only at sites 22 and 32, with values of +0.1 and +0.07 mm/year, respectively. All sites along the Gulf coast show p-values less than 0.05, indicating statistical significance for both negative and positive trends. The predominance of negative trends in wave setup along the Gulf coast is consistent with the spatial pattern of long-term significant wave-height trends inferred from buoy observations in the region (Jamous and Marsooli, 2023).

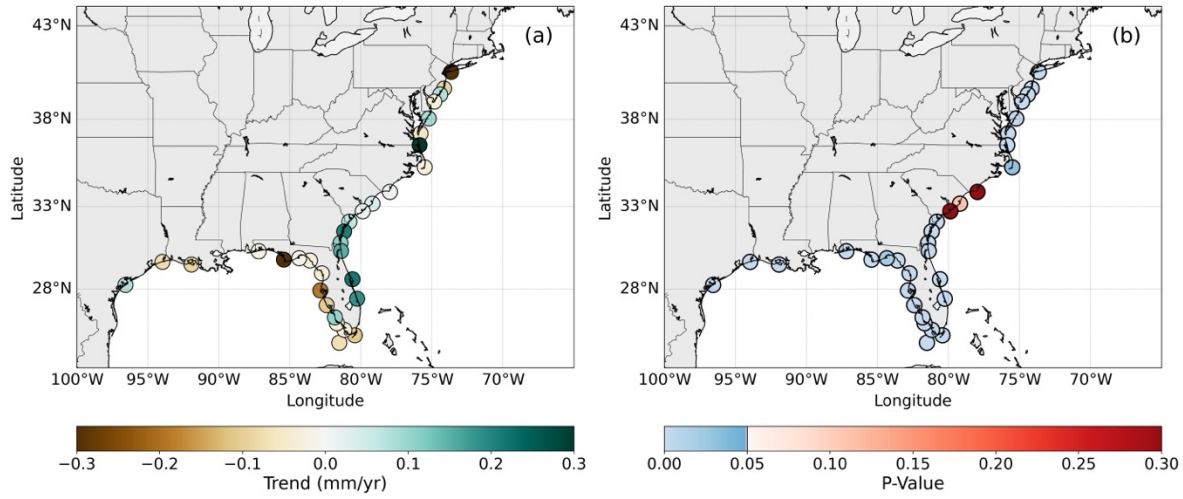

Fig. 7. Trends over the whole time series of wave setup along the U.S. East and Gulf of Mexico coasts for the period of 2006–2015. (a) trend in wave setup (mm yr^{-1}), (b) corresponding p-values.

4. Discussion

Using a coupled hydrodynamic–wave model, this study quantified a decade-long climatology of wave setup along the U.S. East and Gulf coasts, spanning from 2006 to 2015. This addresses the current research gap arising from the reliance on empirical formulation in previous studies of the long-term wave setup climatology (e.g., Melet et al., 2018, 2020). The study is a step forward in advancing our understanding of wave setup climatology by using dynamic modeling.

The results indicate that the open Atlantic coastline consistently experiences higher mean and extreme wave setup than the Gulf of Mexico. The regional differences in wave setup reflect variations in wave climate and nearshore bathymetry. Wave energy along the U.S. East Coast shows a strong spatial gradient across the shore, and the Gulf of Mexico region

has the least wave energy (Yang et al., 2023). The open Atlantic coastline is exposed to larger waves because of greater wind fetch in the open ocean, frequent intense storms, and incoming ocean swells; together these factors produce higher wave setup (Marsooli and Lin, 2018). On the contrary, the Gulf of Mexico is a semi-enclosed basin with limited fetch, therefore, prevailing waves are generally smaller and large-wave events are primarily hurricane-driven (Jamous and Marsooli, 2023), resulting in much lower mean and extreme wave setup at Gulf sites. In the Gulf of Mexico, sites on the western side (sites 30-32) have larger wave setup than the eastern side (19-29). The seasonal winter cold fronts (*nortes)* play an important role in determining the mean wave condition in the Gulf of Mexico, as they produce the strongest extreme wave anomalies along the western Gulf coast (Appendini et al., 2014). This pattern coincides with the results of Maya et al. (2022), who identified that the highest mean wave power is off the west Gulf of Mexico. Differences in nearshore bathymetry further modulate spatial patterns of wave setup along the U.S. East and Gulf of Mexico. Some regions of the Atlantic coast have relatively narrow continental shelves that allow incoming waves to retain more energy until breaking near the shore.

The analysis also shows pronounced seasonal differences, with winter months consistently producing greater wave setup than summer. During winter months, intense and frequent extratropical cyclones result in increased wave activity along the Atlantic coast (Allahdadi et al., 2019). Consequently, the wave setup is higher in winter due to local wind conditions, leading to greater seasonal differences. These large, slow-moving storms can impact the coast for days with powerful northeast winds and high waves, leading to persistently high mean and extreme wave setup. In contrast, summers are relatively calm; outside the hurricane season, fair-weather wave conditions dominate, resulting in much lower wave setup. Along the Atlantic Southeast coast, our results showed that the winter average extreme wave setup is only slightly higher than the summer average, and the ranges overlap considerably, indicating that swells strongly influence wave climatology in this region. During summer, distant hurricanes in the Atlantic Ocean generate powerful swells that propagate toward the coast, elevating coastal water levels (Zheng et al., 2015); consequently, the difference between summer and winter extreme wave setup in this region is not large. The Gulf of Mexico has an overall smaller seasonal difference because of its semi-enclosed geography and limited fetch, which produces generally smaller waves year-round. However, the winter cold fronts (*nortes*) modulate the mean and extreme wave climate (Appendini et al., 2014), and consequently wave setup is higher during winter in this region.

503 The interannual variability of the wave setup along the U.S. East Coast is related to the
504 large-scale climate drivers that modulate the incident wave climate. Year-to-year changes in
505 wave setup correspond to variations in wave energy in the western North Atlantic, which are
506 mainly influenced by the El Niño–Southern Oscillation (ENSO) and Pacific North American
507 (PNA) pattern (Bromirski and Cayan, 2015). La Niña, the cold phase of ENSO, significantly
508 increases tropical cyclone activity in the Atlantic basin due to weaker upper-level westerly
509 winds over the tropical Atlantic, which reduces vertical wind shear (Wang et al., 2025). In
510 addition, El Niño, the warm phase of ENSO, strengthens and shifts the mid-latitude jet stream
511 and storm tracks, which can increase the frequency and intensity of winter extratropical
512 cyclones over the northwest Atlantic (Yang et al., 2018). These mid-latitude westerly storms,
513 together with tropical cyclones, increase the wave power and are the primary sources of the
514 swell that propagates toward the U.S. East Coast.

515 The PNA pattern is another major climate driver linked to U.S. East Coast wave
516 conditions and, thus, the interannual variability in wave setup. The winter wave power along
517 the western boundary of the North Atlantic covaries with the PNA index, indicating that
518 PNA-related changes in the upper-level circulation and storm tracks over North America
519 modulate the frequency and intensity of extratropical cyclones over the northwest Atlantic,
520 and thus the swell energy reaching the U.S. East Coast (Hochet et al., 2021, Bromirski and
521 Cayan, 2015). While the North Atlantic oscillation (NAO) has its strongest impact on wave
522 height in the northeast Atlantic (Santo et al., 2016, Morales-Márquez et al., 2020), negative
523 NAO phases increase cyclogenesis and the frequency of nor'easters (Chartrand and Pausata,
524 2020), and therefore influence swell energy and wave height along the U.S. East Coast,
525 particularly in the northeastern U.S. As a result of these large-scale climate patterns, the
526 interannual variability of mean and extreme wave setup is higher along the U.S. East Coast.
527 Along the Gulf coast, the interannual variability of waves, and consequently the wave setup,
528 is primarily driven by tropical cyclones, winter cold fronts (*nortes*) (Appendini et al., 2014),
529 and remotely generated coastal Kelvin waves (Lin et al., 2014).

530 The spatial variation of our calculated trends in wave setup is consistent with historical
531 trends in significant wave height. Bromirski and Cayan (2015) showed a weak upward trend
532 in both mean significant wave height and wave power in the western North Atlantic. A
533 positive trend of mean significant wave height of 0.5-3.4 cm yr^{-1} is identified between 1950-
534 1990 (Wang and Swail, 2002), and a smaller trend of ±0.1 cm yr^{-1} over the 1990-2020

(Timmermans et al., 2020). This upward trend is attributed primarily to internal variability within the climate system (e.g., interactions among the atmosphere, ocean, and cryosphere) rather than to anthropogenic climate change (Hochet et al., 2023). At the regional scale, long-term and decadal-scale mean significant wave height shows both positive and negative trends along the U.S. East Coast, reflecting the combined influence of basin- to regional-scale forcing and site-specific factors, whereas most sites in the Gulf of Mexico show negative trends. For example, along the U.S. East Coast, Jamous and Marsooli (2023) found an upward trend of mean significant wave height at buoy 44014, located offshore of Virginia Beach, VA. In contrast, buoy 41008, located southeast of Savannah, GA, exhibits a negative trend in mean significant wave height. Similarly, our results indicate a mixed spatial pattern in the emerging trend of wave setup along the U.S. East Coast, and mainly a downward trend in the Gulf of Mexico.

This study has several limitations that introduce uncertainty and suggest directions for future work. One limitation is the model's resolution in the nearshore zone. The study used a coupled hydrodynamic-wave model with a resolution of 500 m to 1 km up to a water depth of 300 m, which may not fully resolve steep bathymetric gradients near shore. Therefore, it prevents the generation of reliable estimates of wave setup at every coastal grid point within the model domain. Despite this limitation, the results provide important insights into the spatial and temporal variability of wave setup at selected sites, where the nearshore bathymetric gradient is gentle.

Another source of uncertainty in our results stems from the accuracy of wave setup estimates that are constrained by the resolution of the model's forcing data, particularly the atmospheric wind and pressure fields from the ERA5 reanalysis. While ERA5 shows the closest agreement with observations among other reanalysis datasets (Wu et al., 2023), biases persist during extreme events due to its finite horizontal resolution of $0.25^{\circ}\times0.25^{\circ}$. ERA5 tends to underestimate the peak winds of intense tropical cyclones and deep extratropical storms, as its coarse grid cannot fully resolve the inner-core structure of these systems, where the strongest winds are concentrated (Hodges et al., 2017). For example, Campos et al. (2022) showed that ERA5 underestimates the surface wind speed by about 8-10% at the 95^{th} and 99^{th} percentiles in the North Atlantic Ocean. Wu et al. (2020) showed that biases in the forcing wind field are strongly reflected in the simulated significant wave height, with underestimates of wind speed leading to corresponding underestimates of significant wave

height. Consequently, extreme wave setup estimates in our study may underestimate the true extremes.

Finally, we acknowledge that a simulation period of more than 10 years will provide a more reliable basis for investigating long-term trends in wave setup. However, due to the substantial computational cost of the simulations, the present study examined the emerging trend in wave setup only at a decade-long scale. As a result, any trend or low-frequency variability inferred from our 10-year (2006-2015) analysis could be strongly influenced by internal climate oscillations or the specific sequence of active and quiet storm seasons during that period, rather than representing a persistent climate-driven change. Overall, our climatological analysis helps locate hotspot segments where wave setup change or variability is most pronounced, and future studies can utilize it to develop site-specific, ultra-high-resolution models and extend the hindcast period to better characterize long-term wave-induced water level changes.

5. Summary and Conclusion

This study investigates a decade-long climatology of wave setup along the U.S. East and Gulf of Mexico Coasts by employing a high-resolution coupled circulation-wave model (ADCIRC + SWAN). A 10-year (2006-2015) hindcast of coastal water levels is generated in the presence and absence of wave effects to compute the wave setup near the coast. To account for the impact of wind-generated waves and swells on coastal water levels, the model is forced at its respective boundary with hourly surface pressure and wind fields, total water level, and direction-frequency wave spectrum data from the ERA5 reanalysis dataset. Across the study domain, 32 representative sites are selected, based on the model grid resolution, to analyze the spatial patterns and temporal variability in wave setup across diverse coastal environments.

The results showed a pronounced spatial and seasonal variation in wave setup. The East Coast consistently experiences larger wave setup than the Gulf of Mexico, reflecting its exposure to more energetic wave climates and steeper continental shelf slopes. The average mean wave setup across Gulf Coast sites is 44% of that averaged across the East Coast sites. Among all sites, the highest extreme (99^{th} percentile) wave setup is found near Virginia Beach, VA (site 7) at 8.19 cm, reflecting the region's exposure to extreme events. When averaged over all sites, extreme wave setup on the Gulf Coast is 48% of that averaged over

East Coast sites. Seasonally, winter months consistently produce higher mean and extreme wave setup than summer months across all regions. This seasonal contrast is most pronounced along the northeast Atlantic coast, where frequent winter nor'easters produce elevated wave setup. Along the southeast coast, this seasonal gap narrows because of the distant storm-generated swells that propagate toward the coast and can elevate water levels during summer as well.

Year-to-year fluctuations in annual mean wave setup were most pronounced at locations with narrow continental shelves and direct exposure to open-ocean wave energy. For example, parts of the Southeast Atlantic (central Florida coast) showed higher interannual variability, reflecting that an active storm year can substantially elevate local wave setup compared to a quiet year. In contrast, sites fronted by broad, shallow continental shelves (e.g., Georgia and South Carolina) experienced much lower interannual variability, as the extended shallow shelves dissipate the wave energy near the coast. Overall, the Atlantic coast exhibits greater interannual variability in annual mean and extreme wave setup than the Gulf by about 57% and 28%, respectively, aligning with the Atlantic's more energetic and swell-dominated wave climate and its more frequent storm activity influenced by large-scale climate patterns.

Beyond temporal variability, the spatial correlation analysis reveals clear regional contrasts in the coherence of wave-setup variability. Wave-setup anomalies showed strong coherence at short alongshore separations (0–75 km) along both the East and Gulf coasts, indicating that nearby coastal segments often respond similarly to shared wave and storm forcing. However, spatial dependence persists over substantially longer distances along the East Coast, with a decorrelation range of approximately 642 km, compared to a much shorter range of about 292 km in the Gulf of Mexico. This difference suggests that wave-setup behavior along the East Coast reflects broader regional coherence, while Gulf Coast variability transitions more quickly from regionally shared to locally differentiated responses.

The estimated 10-year trends in wave setup along the U.S. East Coast were spatially mixed, adjacent sites often showed opposite-signed trends, with no consistent north–south gradient. The largest trend is found at Virginia Beach, VA (site 7) of +0.30 mm/year. In contrast, the Gulf coast shows predominantly negative trends in wave setup over the simulated period. These regional contrasts in trends are consistent with observed long-term changes in wave climate along the U.S. East and Gulf coasts. It is important to note that the

magnitudes of these trends are modest, and a decade is a relatively short period for detecting climate-driven changes in wave setup.

In summary, this study provides the first regional-scale wave setup climatology for the U.S. Atlantic coast based on dynamic modeling. Our results highlight the importance of accounting for wave setup in coastal sea-level assessments and flood risk management. Long-term changes in wave setup can significantly influence high-tide flood forecasting by altering mean sea level anomalies along the coast. Even modest wave-induced increases in coastal water levels can raise high tides above flood thresholds, greatly increasing the frequency of minor high-tide flooding events. Additionally, representing wave setup in sea-level assessments is important because it constitutes a spatially variable contribution to coastal water-level change that can modify both mean conditions and extremes. Overall, incorporating wave setup in flood hazard and sea-level assessments could avoid underestimating coastal water levels and associated long-term flood risks.

Future work can extend this study by conducting a causal analysis to identify the drivers of wave setup variability and their relative importance. Such a causation analysis can build directly on the spatial and seasonal patterns and hotspot segments identified in this study and help determine whether the dominant controls on wave setup variability differ across regions and coastal settings. For example, it can identify the relative importance of variabilities in each wave characteristic, as well as water levels, in explaining the wave setup variabilities. This type of causation analysis would complement the climatological baseline established in this study by translating the identified variability into a clearer physical understanding of its controlling factors.

651 REFERENCES

652 Al Azad, A. A., & Marsooli, R. (2024). A high-resolution coupled circulation-wave model
653 for regional dynamic downscaling of water levels and wind waves in the western North
654 Atlantic ocean. *Ocean Engineering*, *311*, 118869.

655 Allahdadi, M. N., He, R., & Neary, V. S. (2019). Predicting ocean waves along the US east
656 coast during energetic winter storms: Sensitivity to whitecapping parameterizations.
657 *Ocean Science*, 15(3), 691-715.

658 Appendini, C. M., Torres-Freyermuth, A., Salles, P., López-González, J., & Mendoza, E. T.
659 (2014). Wave climate and trends for the Gulf of Mexico: A 30-yr wave hindcast. *Journal*
660 *of Climate*, *27*(4), 1619-1632.

661 Atkinson AL, Power HE, Moura T, Hammond T, Callaghan DP, Baldock TE (2017)
662 Assessment of runup predictions by empirical models on non-truncated beaches on the
663 south-east Australian coast. *Coast Eng* 119:15–31

664 Aucan, J., Hoeke, R. K., Storlazzi, C. D., Stopa, J., Wandres, M., & Lowe, R. (2019). Waves
665 do not contribute to global sea-level rise. *Nature Climate Change*, *9*(1), 2-2.

666 Belknap, D. F., Kelley, J. T., & Gontz, A. M. (2002). Evolution of the glaciated shelf and
667 coastline of the northern Gulf of Maine, USA. *Journal of Coastal Research*, (36), 37-55.

668 Berne, A., Delrieu, G., Creutin, J. D., & Obled, C. (2004). Temporal and spatial resolution of
669 rainfall measurements required for urban hydrology. Journal of Hydrology, 299(3-4),
670 166-179.

671 Birol, F., Léger, F., Passaro, M., Cazenave, A., Niño, F., Calafat, F. M., ... & Benveniste, J.
672 (2021). The X-TRACK/ALES multi-mission processing system: New advances in
673 altimetry towards the coast. *Advances in Space Research*, 67(8), 2398-2415.

674 Boerner, T. J., Deems, S., Furlani, T. R., Knuth, S. L., & Towns, J. (2023). Access:
675 Advancing innovation: Nsf's advanced cyberinfrastructure coordination ecosystem:
676 Services & support. In *Practice and experience in advanced research computing 2023:*
677 *Computing for the common good* (pp. 173-176).

678 Booij, N., Ris, R. C., & Holthuijsen, L. H. (1999). A third-generation wave model for coastal
679 regions. 1: Model description and validation. *Journal of Geophysical*
680 *Research*, **104**(C4), 7649–7666. https://doi.org/10.1029/98JC02622

681 Bowen, A. J., Inman, D. L., & Simmons, V. P. (1968). Wave 'set-down' and set-up. *Journal*
682 *of geophysical research*, *73*(8), 2569-2577.

683 Bromirski, P. D., & Cayan, D. R. (2015). Wave power variability and trends across the North
684 Atlantic influenced by decadal climate patterns. *Journal of Geophysical Research:*
685 *Oceans*, *120*(5), 3419-3443.

686 Campos, R. M., Gramcianinov, C. B., de Camargo, R., & da Silva Dias, P. L. (2022).
687 Assessment and calibration of ERA5 severe winds in the Atlantic Ocean using satellite
688 data. *Remote Sensing*, *14*(19), 4918.

689 Camus, P., Mendez, F. J., Medina, R., Tomas, A., & Izaguirre, C. (2013). High resolution
690 downscaled ocean waves (DOW) reanalysis in coastal areas. *Coastal Engineering*, 72, 56-
691 68.

692 Casas-Prat, M., Hemer, M. A., Dodet, G., Morim, J., Wang, X. L., Mori, N., ... & Feng, Y.
693 (2024). Wind-wave climate changes and their impacts. *Nature Reviews Earth &*
694 *Environment*, *5*(1), 23-42.

695 Chartrand, J., & Pausata, F. S. R. (2020). Impacts of the North Atlantic Oscillation on Winter
696 Precipitations and Storm Track Variability in Southeast Canada and Northeast
697 US. *Weather and Climate Dynamics Discussions*, *2020*, 1-24.

698 Cressie, N. A.: Statistics for spatial data, Wiley, NY, revised edn., 1993. 2090.

699 Dean, B., Collins, I., Divoky, D., Hatheway, D., & Scheffner, C. N. (2005). *FEMA coastal*
700 *flood hazard analysis and mapping guidelines focused study report*. Tech. rep.

701 Diaz-Maya, M., Ulloa, M., & Silva, R. (2022). Assessing wave energy converters in the gulf
702 of Mexico using a multi-criteria approach. *Frontiers in Energy Research*, *10*, 929625.

703 Dietrich, J. C., Zijlema, M., Westerink, J. J., Holthuijsen, L. H., Dawson, C., Luettich Jr, R.
704 A., ... & Stone, G. W. (2011). Modeling hurricane waves and storm surge using
705 integrally-coupled, scalable computations. *Coastal Engineering*, *58*(1), 45-65.

706 Dietrich, J. C., Tanaka, S., Westerink, J. J., Dawson, C. N., Luettich Jr, R. A., Zijlema, M., ...
707 & Westerink, H. J. (2012). Performance of the unstructured-mesh, SWAN+ ADCIRC
708 model in computing hurricane waves and surge. Journal of Scientific Computing, 52(2),
709 468-497.

Dodet, G., Melet, A., Ardhuin, F., Bertin, X., Idier, D., & Almar, R. (2019). The contribution of wind-generated waves to coastal sea-level changes. *Surveys in Geophysics*, *40*(6), 1563-1601.

Dodet, G., Melet, A., Ardhuin, F., Bertin, X., Idier, D., & Almar, R. (2019). The contribution of wind-generated waves to coastal sea-level changes. *Surveys in Geophysics*, *40*(6), 1563-1601.

Dodet, G., Melet, A., Ardhuin, F., Bertin, X., Idier, D., & Almar, R. (2019). The contribution of wind-generated waves to coastal sea-level changes. *Surveys in Geophysics*, *40*(6), 1563-1601.

Haasnoot, M., Winter, G., Brown, S., Dawson, R. J., Ward, P. J., & Eilander, D. (2021). Long-term sea-level rise necessitates a commitment to adaptation: A first order assessment. *Climate Risk Management*, *34*, 100355.

Heidarzadeh, M., Teeuw, R., Day, S., & Solana, C. (2018). Storm wave runups and sea level variations for the September 2017 Hurricane Maria along the coast of Dominica, eastern Caribbean sea: Evidence from field surveys and sea-level data analysis. *Coastal Engineering Journal*, *60*(3), 371-384.

Hersbach, H., Bell, B., Berrisford, P., Hirahara, S., Horányi, A., Muñoz-Sabater, J., ... & Thépaut, J. N. (2020). The ERA5 global reanalysis. *Quarterly journal of the royal meteorological society*, *146*(730), 1999-2049.

Hochet, A., Dodet, G., Ardhuin, F., Hemer, M., & Young, I. (2021). Sea state decadal variability in the North Atlantic: A review. *Climate*, *9*(12), 173.

Hochet, A., Dodet, G., Sévellec, F., Bouin, M. N., Patra, A., & Ardhuin, F. (2023). Time of emergence for altimetry-based significant wave height changes in the North Atlantic. *Geophysical Research Letters*, *50*(9), e2022GL102348.

Hodges, K., Cobb, A., & Vidale, P. L. (2017). How well are tropical cyclones represented in reanalysis datasets? *Journal of Climate*, *30*(14), 5243-5264.

Holman RA, Sallenger AH Jr (1985) Setup and Swash on a natural beach. J Geophys Res 90(C1):945–953

738 Jamous, M., & Marsooli, R. (2023). A Multidecadal Assessment of Mean and Extreme Wave
739 Climate Observed at Buoys off the US East, Gulf, and West Coasts. *Journal of Marine*
740 *Science and Engineering*, *11*(5), 916.

741 Lentz, S., & Raubenheimer, B. (1999). Field observations of wave setup. *Journal of*
742 *Geophysical Research: Oceans*, *104*(C11), 25867-25875.

743 Li, N., Cheung, K. F., Stopa, J. E., Hsiao, F., Chen, Y. L., Vega, L., & Cross, P. (2016).
744 Thirty-four years of Hawaii wave hindcast from downscaling of climate forecast system
745 reanalysis. Ocean Modelling, 100, 78-95.

746 Lin, N., Lane, P., Emanuel, K. A., Sullivan, R. M., & Donnelly, J. P. (2014). Heightened
747 hurricane surge risk in northwest Florida revealed from climatological-hydrodynamic
748 modeling and paleorecord reconstruction. *Journal of Geophysical Research:*
749 *Atmospheres*, *119*(14), 8606-8623.

750 Longuet-Higgins, M. S., & Stewart, R. W. (1962). Radiation stress and mass transport in
751 gravity waves, with application to 'surf beats'. *Journal of Fluid Mechanics*, *13*(4), 481-
752 504.

753 Longuet-Higgins, M. S., & Stewart, R. W. (1964, August). Radiation stresses in water waves;
754 a physical discussion, with applications. In Deep sea research and oceanographic
755 abstracts (Vol. 11, No. 4, pp. 529-562). Elsevier.

756 Luettich, R. A., Westerink, J. J., & Scheffner, N. W. (1992). ADCIRC: an advanced three-
757 dimensional circulation model for shelves, coasts, and estuaries. Report 1, Theory and
758 methodology of ADCIRC-2DD1 and ADCIRC-3DL.

759 Marsooli, R., & Lin, N. (2018). Numerical modeling of historical storm tides and waves and
760 their interactions along the US East and Gulf Coasts. Journal of Geophysical Research:
761 Oceans, 123(5), 3844-3874.

762 Marsooli, R., Orton, P. M., Mellor, G., Georgas, N., & Blumberg, A. F. (2017). A coupled
763 circulation–wave model for numerical simulation of storm tides and waves. *Journal of*
764 *Atmospheric and Oceanic Technology*, *34*(7), 1449-1467.

765 Melet, A., Almar, R., & Meyssignac, B. (2016). What dominates sea level at the coast: a case
766 study for the Gulf of Guinea. *Ocean Dynamics*, *66*, 623-636.

767 Melet, A., Almar, R., Hemer, M., Le Cozannet, G., Meyssignac, B., & Ruggiero, P. (2020).
768 Contribution of wave setup to projected coastal sea level changes. *Journal of Geophysical*
769 *Research: Oceans*, *125*(8), e2020JC016078.

770 Melet, A., Meyssignac, B., Almar, R., & Le Cozannet, G. (2018). Under-estimated wave
771 contribution to coastal sea-level rise. *Nature Climate Change*, *8*(3), 234-239.

772 Melet, A., Meyssignac, B., Almar, R., & Le Cozannet, G. (2018). Under-estimated wave
773 contribution to coastal sea-level rise. *Nature Climate Change*, *8*(3), 234-239.

774 Morales-Márquez, V., Orfila, A., Simarro, G., & Marcos, M. (2020). Extreme waves and
775 climatic patterns of variability in the eastern North Atlantic and Mediterranean
776 basins. *Ocean Science Discussions*, *2020*, 1-21.

777 Pedreros, R., Idier, D., Muller, H., Lecacheux, S., Paris, F., Yates-Michelin, M., ... &
778 Senechal, N. (2018). Relative contribution of wave setup to the storm surge: observations
779 and modeling based analysis in open and protected environments (Truc Vert beach and
780 Tubuai island). *Journal of Coastal Research*, (85), 1046-1050.

781 Raubenheimer, B., Guza, R. T., & Elgar, S. (2001). Field observations of wave-driven
782 setdown and setup. *Journal of Geophysical Research: Oceans*, *106*(C3), 4629-4638.

783 Ray, R. D., Merrifield, M. A., & Woodworth, P. L. (2023). Wave setup at the
784 Minamitorishima tide gauge. *Journal of Oceanography*, *79*(1), 13-26.

785 Ris, R. C., Holthuijsen, L. H., & Booij, N. (1999). A third-generation wave model for coastal
786 regions: 2.Verification. *Journal of Geophysical Research*, **104**(C4), 7649–
787 7666. https://doi.org/10.1029/1998JC900123

788 Rueda, A., Vitousek, S., Camus, P., Tomás, A., Espejo, A., Losada, I. J., ... & Mendez, F. J.
789 (2017). A global classification of coastal flood hazard climates associated with large-scale
790 oceanographic forcing. *Scientific reports*, *7*(1), 5038.

791 Ruggiero, P. (2013). Is the intensifying wave climate of the US Pacific Northwest increasing
792 flooding and erosion risk faster than sea-level rise?. *Journal of Waterway, Port, Coastal,*
793 *and Ocean Engineering*, *139*(2), 88-97.

794 Santo, H., Taylor, P. H., & Gibson, R. (2016). Decadal variability of extreme wave height
795 representing storm severity in the northeast Atlantic and North Sea since the foundation

of the Royal Society. *Proceedings of the Royal Society A: Mathematical, Physical and Engineering Sciences*, *472*(2193), 20160376.

Schlembach, F., Ehlers, F., Kleinherenbrink, M., Passaro, M., Dettmering, D., Seitz, F., & Slobbe, C. (2023). Benefits of fully focused SAR altimetry to coastal wave height estimates: A case study in the North Sea. Remote Sensing of Environment, 289, 113517.

Serafin, K. A., Ruggiero, P., & Stockdon, H. F. (2017). The relative contribution of waves, tides, and nontidal residuals to extreme total water levels on US West Coast sandy beaches. *Geophysical Research Letters*, *44*(4), 1839-1847.

Stockdon HF, Holman RA, Howd PA, Sallenger AH Jr (2006) Empirical parameterization of setup, swash, and runup. *Coast Eng* 53:573–588.https://doi.org/10.1016/j.coastaleng.2005.12.005

Swail, V. R., Wang, X. L., & Cox, A. T. (2002, October). The wave climate of the North Atlantic—Past, present and future. In *Proceedings of the 7th international workshop on wave hindcasting and forecasting* (p. 12).

Timmermans, B. W., Gommenginger, C. P., Dodet, G., & Bidlot, J. R. (2020). Global wave height trends and variability from new multimission satellite altimeter products, reanalyses, and wave buoys. *Geophysical Research Letters*, *47*(9), e2019GL086880.

Vitousek, S., Barnard, P. L., Fletcher, C. H., Frazer, N., Erikson, L., & Storlazzi, C. D. (2017). Doubling of coastal flooding frequency within decades due to sea-level rise. *Scientific reports*, *7*(1), 1399.

Wang, X., Quan, M., & Fan, K. (2025). Effects of El Niño–Southern Oscillation Dissipation Phases on Tropical Cyclone Activity over the North Atlantic. *Ocean-Land-Atmosphere Research*, *4*, 0082.

Westerink, J. J., Luettich Jr, R. A., & Muccino, J. C. (1994). Modelling tides in the western North Atlantic using unstructured graded grids. *Tellus A*, *46*(2), 178-199.

Woodworth, P. L., Melet, A., Marcos, M., Ray, R. D., Wöppelmann, G., Sasaki, Y. N., ... & Merrifield, M. A. (2019). Forcing factors affecting sea level changes at the coast. *Surveys in Geophysics*, *40*(6), 1351-1397.

824 Woodworth, P. L., Melet, A., Marcos, M., Ray, R. D., Wöppelmann, G., Sasaki, Y. N., ... &
825 Merrifield, M. A. (2019). Forcing factors affecting sea level changes at the coast. *Surveys*
826 *in Geophysics*, *40*(6), 1351-1397.

827 Wu, L., Su, H., Zeng, X., Posselt, D. J., Wong, S., Chen, S., & Stoffelen, A. (2024).
828 Uncertainty of atmospheric winds in three widely used global reanalysis datasets. *Journal*
829 *of Applied Meteorology and Climatology*, *63*(2), 165-180.

830 Wu, W., Li, P., Zhai, F., Gu, Y., & Liu, Z. (2020). Evaluation of different wind resources in
831 simulating wave height for the Bohai, Yellow, and East China Seas (BYES) with SWAN
832 model. *Continental Shelf Research*, *207*, 104217.

833 Yang, S., Li, Z., Yu, J. Y., Hu, X., Dong, W., & He, S. (2018). El Niño–Southern Oscillation
834 and its impact in the changing climate. *National Science Review*, *5*(6), 840-857.

835 Yang, Z., Medina, G. G., Neary, V. S., Ahn, S., Kilcher, L., & Bharath, A. (2023). Multi-
836 decade high-resolution regional hindcasts for wave energy resource characterization in
837 US coastal waters. *Renewable Energy*, *212*, 803-817.

838 Zheng, K., Sun, J., Guan, C., & Shao, W. (2016). Analysis of the global swell and wind sea
839 energy distribution using WAVEWATCH III. *Advances in Meteorology*, *2016*(1),
840 8419580.

Statements & Declarations

Competing interests

The authors have no relevant financial or nonfinancial interests to disclose.

Author Contributions

All authors contributed to the study conception and design. Methodology, investigation, formal analysis, data curation, and visualization were performed by ASM Alauddin Al Azad. Reza Marsooli provided supervision and contributed to conceptualization, methodology, investigation. The first draft of the manuscript was written by ASM Alauddin Al Azad and all authors commented on previous versions of the manuscript. All authors read and approved the final manuscript.

Data Availability

Bathymetric data for the model domain were obtained from GEBCO 2021 and are available from the GEBCO portal (www.gebco.net). ERA5 reanalysis data can be downloaded from the Copernicus climate data store (cds.climate.copernicus.eu/datasets/). The wave setup estimates produced in this study are available upon request by email to the corresponding author.

Acknowledgments.

This work used Purdue Anvil CPU resource at Purdue University through allocation #EES240038 from the **Advanced Cyberinfrastructure Coordination Ecosystem: Services & Support** (ACCESS) program, which is supported by U.S. National Science Foundation grants #2138259, #2138286, #2138307, #2137603, and #2138296.